RUB-TPII-11/95

# Update of the stranger story: The strange vector form factors of the nucleon in the SU(3) chiral quark-soliton model

Hyun-Chul Kim *, Teruaki Watabe †, and Klaus Goeke ‡

*Institut für Theoretische Physik II,*

*Postfach 102148, Ruhr-Universität Bochum,*

*D–44780 Bochum, Germany*

(March 1996)

## Abstract

The strange vector form factors are evaluated for $Q^2 = 0$ and $Q^2 = 1$ GeV$^2$ in the framework of the SU(3) chiral quark-soliton model (or semi-bosonized SU(3) Nambu-Jona-Lasinio model). The rotational $1/N_c$ and $m_s$ corrections are taken into account up to linear order. The mean-square strange radius $\langle r^2 \rangle_s^{Sachs} = -0.35$ fm$^2$ and the strange magnetic moment $\mu_s = -0.44\ \mu_N$ are obtained. The results are compared with several different models.

PACS: 12.40.-y, 14.20.Dh



*E-mail address: kim@hadron.tp2.ruhr-uni-bochum.de

†E-mail address: watabe@hadron.tp2.ruhr-uni-bochum.de

‡E-mail address: goeke@hadron.tp2.ruhr-uni-bochum.de

## I. INTRODUCTION

The strangeness content of the nucleon has been under a great deal of discussions for well over a decade. A few years ago, the European Muon Collaboration (EMC) [1] measured the spin structure function of the proton in deep inelastic muon scattering and showed that there is an indication of a sizable strange quark contribution. This remarkable result has been confirmed by following experiments of the Spin Muon Collaboration (SMC) [2,3], E142 and E143 collaborations [4,5].

Another experiment conducted at Brookhaven [6] (BNL experiment 734) measuring the low-energy elastic neutrino-proton scattering came to the more or less same conclusion. Kaplan and Manohar [7] showed how elastic $\nu p$ and $ep$ scatterings can be used to extract not only the $G_1$ form factors of the $U(1)_A$ current but also the $F_2$ form factors of the baryon number current and furthermore how the strange quark matrix elements $\langle p|\bar{s}\gamma_\mu\gamma_5 s|p\rangle$ and $\langle p|\bar{s}\gamma_\mu s|p\rangle$ can be evaluated. Following these suggestions, Garvey *et al.* [8] reanalyzed the above-mentioned $\nu p$ elastic scattering experiment and determined proton strange form factors in particular at $Q^2 = 0$, pointing out the shortcomings of the analysis done by Ref. [6] . The best fit of Ref. [8] with the smallest $\chi^2$ tells $F_1^s = 0.53 \pm 0.70$ and $F_2^s = -0.40 \pm 0.72$. By comparing the different $Q^2$ dependence of $d\sigma/dQ^2(\nu p)$ to $d\sigma/dQ^2(\bar{\nu}p)$, Garvey *et al.* favor $F_1^s(Q^2) > 0$ and $F_2^s(Q^2) < 0$. However, these form factors are experimentally unknown to date and have no stringent and concrete constraints on their $Q^2$–dependence yet. There are various proposals and experiments in progress (see Refs. [19,20] for details). All these considerations lead to the conclusion that, in contrast to the naive quark model, it is of great importance to consider strange quarks in the nucleon seriously.

There have been several theoretical efforts to describe the strange form factors of the nucleon. The first attempt was performed by Jaffe [9]. Jaffe took advantage of Ref. [10], *i.e.* the pole fit analysis based on dispersion theory and estimated the mean-square strange radius and magnetic moment of the nucleon:$\langle r^2\rangle_s^{Dirac} = 0.16 \pm 0.06$ fm$^2$, $\mu_s = -0.31 \pm 0.09\ \mu_N$. More recently, Hammer *et al.* [11] updated Jaffe's pole-fit analysis of the strange vector form

factors, relying upon a new dispersion theoretic analysis of the nucleon electromagnetic form factors. In fact, Hammer *et al.* improved Jaffe's prediction, giving $\mu_s = -0.24 \pm 0.03\ \mu_N$ and $\langle r^2 \rangle_s^{Dirac} = 0.21 \pm 0.03$ fm$^2$. A noticeable point of the pole-fit analysis is that it has the different sign of the strange electric radius, compared with almost other models.

Another interesting approach is the kaon-loop calculation. The main idea of the kaon-loop calculation is that the strangeness content of the nucleon exists as a pair of $K\Lambda$ or $K\Sigma$ components. Koepf *et al.* [12] first evaluated $\mu_s$ and $\langle r^2 \rangle_s^{Dirac}$, considering the possible kaon loops relevant for the strange vector form factors. However, Ref. [12] failed to include *seagull* terms which are essential to satisfy the Ward-Takahashi identity in the vector current sector. Musolf *et al.* [13] added these seagull terms and obtained $\mu_s = -(0.31 \to 0.40)\ \mu_N$ and $\langle r^2 \rangle_s^{Dirac} = -(6.68 \to 6.90) \times 10^{-3}$ fm$^2$. The prediction of $\langle r^2 \rangle_s^{Dirac}$ in the kaon-loop calculation is found to be much smaller than the pole-fit analysis. To reconcile the conflict between the pole-fit analysis and the kaon-loop calculation, Refs. [14,18] suggested the combination of the vector meson dominance (VMD) and $\omega - \phi$ mixing in the vector-isovector channel with the kaon-loop calculation. The value of $\langle r^2 \rangle_s^{Dirac}$ in Ref. [14] appeared to be larger than that of the kaon-loop calculation but still conspicuosly smaller than that of the pole-fit analysis: $\langle r^2 \rangle_s^{Dirac} = -(2.42 \to 2.45) \times 10^{-2}$ fm$^2$. Ref. [18] evaluated also the strange vector form factors and discussed to a great extent several different theoretical estimates.

The SU(3) Skyrme model with pseudoscalar mesons [15] and with vector mesons [16] estimated, respectively, $\mu_s = -0.13$, $\mu_s = -0.05$ and $\langle r^2 \rangle_s^{Dirac} = -0.10$ fm$^2$, $\langle r^2 \rangle_s^{Dirac} = 0.05$ fm$^2$. Most recently, Leinweber obtained $\mu_s = -0.75 \pm 0.30\ \mu_N$ which appears to be much larger than other models.

In this paper, we aim at investigating the strange vector form factors and related strange observables in the SU(3) chiral quark-soliton model ($\chi$QSM), often called semi-bosonized SU(3) Nambu-Jona-Lasinio model (NJL). The model is based on the interaction of quarks with Goldstone bosons and has been shown to be quite successful in reproducing static properties of the baryons such as mass splitting [21,22], axial constants [23] and magnetic moments [24] and their form factors [25,26]. In a recent review [27], one can easily see how

well the model describe the baryonic observables. In particular, since the strange vector form factors are deeply related to the electromagnetic form factors [9,11] being well described in $\chi$QSM, it is quite interesting to study them in the same framework.

The outline of the paper is as follows: Section II develops the general formalism for obtaining the strange vector form factors in the framework of $\chi$QSM. Section III presents the corresponding results and discuss them. Section IV contains a summary and draws the conclusion of the present work.

## II. GENERAL FORMALISM

In this section we briefly review the formalism of $\chi$QSM. Details can be found in ref. [27]. We start with the low-energy partition function in Euclidean space given by the functional integral over pseudoscalar meson ($\pi^a$) and quark fields($\psi$):

$$\begin{aligned} \mathcal{Z} &= \int \mathcal{D}\psi\mathcal{D}\psi^\dagger\mathcal{D}\pi^a \exp\Big(-\int d^4x\psi^\dagger iD\psi\Big), \\ &= \int \mathcal{D}\pi^a \exp\left(-S_{eff}[\pi]\right), \end{aligned} \tag{1}$$

where $S_{eff}$ is the effective action

$$S_{eff}[\pi] \;=\; -\mathrm{Spln}iD. \tag{2}$$

$iD$ represents the Dirac differential operator

$$iD \;=\; \beta(-i\partial\!\!\!/ + \hat{m} + MU^{\gamma^5}) \tag{3}$$

with the pseudoscalar chiral field

$$U^{\gamma_5} \;=\; \exp\left(i\pi^a\lambda^a\gamma_5\right) \;=\; \frac{1+\gamma_5}{2}U + \frac{1-\gamma_5}{2}U^\dagger. \tag{4}$$

$\hat{m}$ is the matrix of the current quark mass given by

$$\hat{m} \;=\; \mathrm{diag}(m_u, m_d, m_s) \;=\; m_0\mathbf{1} \;+\; m_8\lambda_8, \tag{5}$$

where $\lambda^a$ designate the usual Gell-Mann matrices normalized as $\mathrm{tr}(\lambda^a\lambda^b) = 2\delta^{ab}$. Here, we have assumed isospin symmetry ($m_u = m_d$). $M$ stands for the dynamical quark mass arising from the spontaneous chiral symmetry breaking, which is in general momentum-dependent [28]. We regard $M$ as a constant and introduce the proper-time regularization for convenience. The $m_0$ and $m_8$ in Eq. (5) are defined, respectively, by

$$m_0 \;=\; \frac{m_u + m_d + m_s}{3}, \qquad m_8 \;=\; \frac{m_u + m_d - 2m_s}{2\sqrt{3}}. \tag{6}$$

The operator $iD$ is expressed in Euclidean space in terms of the Euclidean time derivative $\partial_\tau$ and the Dirac one–particle Hamiltonian $H(U^{\gamma_5})$

$$iD \;=\; \partial_\tau \;+\; H(U^{\gamma_5}) + \beta\hat{m} - \beta\bar{m}\mathbf{1} \tag{7}$$

with

$$H(U^{\gamma_5}) \;=\; \frac{\vec{\alpha}\cdot\nabla}{i} \;+\; \beta M U^{\gamma_5} \;+\; \beta\bar{m}\mathbf{1}. \tag{8}$$

$\bar{m}$ is defined by $(m_u + m_d)/2 = m_u = m_d$. $\beta$ and $\vec{\alpha}$ are the well–known Dirac Hermitian matrices. The $U$ is assumed to have a structure corresponding to the so-called trivial embedding of the SU(2)-hedgehog into SU(3):

$$U \;=\; \begin{pmatrix} U_0 & 0 \\ 0 & 1 \end{pmatrix}, \tag{9}$$

with

$$U_0 \;=\; \exp\left[i\vec{n}\cdot\vec{\tau}P(r)\right]. \tag{10}$$

The profile function $P(r)$ is determined numerically by solving the Euler-Lagrange equation corresponding to $\frac{\delta S_{eff}}{\delta P(r)} = 0$. This yields a selfconsistent classical field $U_0$ and a set of single quark energies and corresponding states $E_n$ and $\Psi_n$. Note that the $E_n$ and $\Psi_n$ do not constitute the nucleon $|N\rangle$ yet because the collective spin and and isospin quantum numbers are missing. Those are obtained by the semiclassical quantization procedure, described below in the context of the strange form factors.

The information of the strange vector form factors in the nucleon is contained in the quark matrix elements as follows:

$$\langle N'(p')|J^s_\mu|N(p)\rangle \;=\; \langle N'(p')|\bar{s}\gamma_\mu s|N(p)\rangle. \tag{11}$$

The strange Dirac form factors of the nucleon are defined by the matrix elements of the $J^s_\mu$:

$$\langle N'(p')|J^s_\mu|N(p)\rangle \;=\; \bar{u}_N(p')\left[\gamma_\mu F_1^s(q^2) + i\sigma_{\mu\nu}\frac{q^\nu}{2M_N}F_2^s(q^2)\right]u_N(p), \tag{12}$$

where $q^2$ is the square of the four momentum transfer $q^2 = -Q^2$ with $Q^2 > 0$. $M_N$ and $u_N(p)$ stand for the nucleon mass and its spinor, respectively. The strange quark current $J^s_\mu$ can be expressed in terms of the baryon current and the hypercharge current:

$$J^s_\mu \;=\; \bar{s}\gamma_\mu s \;=\; J^B_\mu - J^Y_\mu \;=\; \bar{q}\gamma_\mu\hat{Q}_s q, \tag{13}$$

where

$$\begin{aligned} J^B_\mu &= \frac{1}{N_c}\bar{q}\gamma_\mu q, \\ J^Y_\mu &= \frac{1}{\sqrt{3}}\bar{q}\gamma_\mu\lambda_8 q \\ \hat{Q}_s &= \frac{1}{N_c} - \frac{1}{\sqrt{3}}\lambda_8, \end{aligned} \tag{14}$$

where $N_c$ denotes the number of colors of the quark. $\hat{Q}_s = \mathrm{diag}(0,0,1)$ is called *strangeness operator*. We employ the non-standard sign convention used by Jaffe [9] for the strange current. The baryon and hypercharge currents are equal to the singlet and octet currents, respectively.

The strange Dirac form factors $F_1^s$ and $F_2^s$ can be written in terms of the strange Sachs form factors, $G_E^s(Q^2)$ and $G_M^s(Q^2)$:

$$\begin{aligned} G_E^s(Q^2) &= F_1^s(Q^2) - \frac{Q^2}{4M_N^2}F_2^s(Q^2) \\ G_M^s(Q^2) &= F_1^s(Q^2) + F_2^s(Q^2). \end{aligned} \tag{15}$$

In the non–relativistic limit($Q^2 \ll M_N^2$), the Sachs-type form factors $G_E^s(Q^2)$ and $G_M^s(Q^2)$ are related to the time and space components of the strange current, respectively:

$$\langle N'(p')|J_0^s(0)|N(p)\rangle = G_E^s(Q^2)$$
$$\langle N'(p')|J_i^s(0)|N(p)\rangle = \frac{1}{2M_N}G_M^s(Q^2)i\epsilon_{ijk}q^j\langle\lambda'|\sigma_k|\lambda\rangle, \tag{16}$$

where $\sigma_k$ stand for Pauli spin matrices. The $|\lambda\rangle$ is the corresponding spin state of the nucleon. The matrix elements of the strange quark current can be related to a correlator:

$$\langle N'(p')|\bar{s}\gamma_\mu s|N(p)\rangle \underset{T\to\infty}{\sim}\langle 0|J_{N'}(\vec{x},T/2)\bar{q}\gamma_\mu\hat{Q}_s q J_N^\dagger(\vec{y},-T/2)|0\rangle. \tag{17}$$

The nucleon current $J_N$ can be built from $N_c$ quark fields

$$J_N(x) \;=\; \frac{1}{N_c!}\epsilon_{i_1\cdots i_{N_c}}\Gamma^{\alpha_1\cdots\alpha_{N_c}}_{JJ_3TT_3Y}\psi_{\alpha_1 i_1}(x)\cdots\psi_{\alpha_{N_c}i_{N_c}}(x). \tag{18}$$

$\alpha_1\cdots\alpha_{N_c}$ denote spin–flavor indices, while $i_1\cdots i_{N_c}$ designate color indices. The matrices $\Gamma^{\alpha_1\cdots\alpha_{N_c}}_{JJ_3TT_3Y}$ are taken to endow the corresponding current with the quantum numbers $JJ_3TT_3Y$. In our model, Eq. (17) is represented by the Euclidean functional integral with regards to quark and pseudo-Goldstone fields:

$$\begin{aligned}\langle N'(p')|\bar{q}\gamma_\mu\hat{Q}_s q|N(p)\rangle = \frac{1}{\mathcal{Z}}\lim_{T\to\infty}\exp\left(ip_4\frac{T}{2}-ip'_4\frac{T}{2}\right)&\\ \times\int d^3x d^3y\exp\left(-i\vec{p'}\cdot\vec{y}+i\vec{p}\cdot\vec{x}\right)\int\mathcal{D}U\int\mathcal{D}\psi\int\mathcal{D}\psi^\dagger&\\ \times\;\; J_{N'}(\vec{y},T/2)q^\dagger(0)\beta\gamma_\mu\hat{Q}_s q(0)J_N^\dagger(\vec{x},-T/2)&\\ \times\exp\left[-\int d^4z\psi^\dagger iD\psi\right],&\end{aligned} \tag{19}$$

where $\mathcal{Z}$ stands for the normalization factor which is expressed by the same functional integral but without the quark current operator $\bar{s}\gamma_\mu s$. Since $\bar{m}$ is much smaller than $m_s$, we use $\hat{m}-\bar{m}\mathbf{1}\simeq diag(0,0,m_s)$ in the perturbation. Eq.(19) can be decomposed into valence and sea contributions:

$$\langle N'(p')|\bar{q}\gamma_\mu\hat{Q}_s q|N(p)\rangle \;=\; \langle N'(p')|\bar{q}\gamma_\mu\hat{Q}_s q|N(p)\rangle_{val} \;+\; \langle N'(p')|\bar{q}\gamma_\mu\hat{Q}_s q|N(p)\rangle_{sea}, \tag{20}$$

where

$$\langle N'(p')|V_\mu(0)|N(p)\rangle_{val} = \frac{1}{\mathcal{Z}}\Gamma^{\beta_1\cdots\beta_{N_c}}_{J'J'_3T'T'_3Y'}\Gamma^{\alpha_1\cdots\alpha_{N_c}*}_{JJ_3TT_3Y}\lim_{T\to\infty}\exp\left(ip_4\frac{T}{2}-ip'_4\frac{T}{2}\right)$$

$$\times \int d^3x d^3y \exp\left(-i\vec{p'}\cdot\vec{y} + i\vec{p}\cdot\vec{x}\right)$$
$$\times \int \mathcal{D}U \exp\left(-S_{eff}\right) \sum_{i=1}^{N_c} {}_{\beta_i}\langle \vec{y}, \mathrm{T}/2|\frac{1}{iD}|0, t_z\rangle_\gamma [\beta\gamma_\mu \hat{Q}_s]_{\gamma\gamma'}$$
$$\times {}_{\gamma'}\langle 0, t_z|\frac{1}{iD}|\vec{x}, -\mathrm{T}/2\rangle_{\alpha_i} \prod_{j\neq i}^{N_c} {}_{\beta_j}\langle \vec{y}, \mathrm{T}/2|\frac{1}{iD}|\vec{x}, -\mathrm{T}/2\rangle_{\alpha_j} \qquad (21)$$

and

$$\langle N'(p')|V_\mu(0)|N(p)\rangle_{sea} = -\frac{N_c}{\mathcal{Z}}\Gamma^{\beta_1\cdots\beta_{N_c}}_{J'J'_3T'T'_3Y'}\Gamma^{\alpha_1\cdots\alpha_{N_c}*}_{JJ_3TT_3Y} \lim_{T\to\infty} \exp\left(ip_4\frac{T}{2} - ip'_4\frac{T}{2}\right)$$
$$\times \int d^3x d^3y \exp\left(-i\vec{p'}\cdot\vec{y} + i\vec{p}\cdot\vec{x}\right)$$
$$\times \int \mathcal{D}U \exp\left(-S_{eff}\right) \mathrm{Tr}\ {}_{\gamma\lambda}\langle 0, t_z|\frac{1}{iD}[\beta\gamma_\mu]\hat{Q}_s|0, t_z\rangle$$
$$\times \prod_{i=1}^{N_c} {}_{\beta_i}\langle \vec{y}, \mathrm{T}/2|\frac{1}{iD}|\vec{x}, -\mathrm{T}/2\rangle_{\alpha_i}. \qquad (22)$$

$S_{eff}$ is the effective chiral action expressed by

$$S_{eff} \;=\; -N_c \mathrm{Spln}\left[\partial_\tau \;+\; H(U^{\gamma_5}) \;+\; \beta\hat{m} \;-\; \beta\bar{m}\mathbf{1}\right]. \qquad (23)$$

In order to perform the collective quantization, we have to integrate Eqs. (21) and (22) over small oscillations of the pseudo-Goldstone field around the saddle point Eq. (9). This will not be done except for the zero modes. The corresponding fluctuations of the pion fields are not small and hence cannot be neglected. The zero modes are relevant to continuous symmetries in our problem. In particular, we have to take into account the translational zero modes properly in order to evaluate form factors, since the soliton is not invariant under translation and its translational invariance is restored only after integrating over the translational zero modes. Explicitly, the zero modes are taken into account by considering a slowly *rotating* and *translating* hedgehog:

$$\tilde{U}(\vec{x}, t) \;=\; A(t)U(\vec{x} - \vec{Z}(t))A^\dagger(t). \qquad (24)$$

$A(t)$ belongs to an SU(3) unitary matrix. The Dirac operator $i\tilde{D}$ in Eq. (7) can be written as

$$i\tilde{D} \;=\; \left(\partial_\tau \;+\; H(U^{\gamma_5}) \;+\; A^\dagger(t)\dot{A}(t) \;-\; i\beta\dot{\vec{Z}}\cdot\nabla \;+\; \beta A^\dagger(t)(\hat{m} - \bar{m}\mathbf{1})A(t)\right). \qquad (25)$$

The corresponding collective action is expressed by

$$\tilde{S}_{eff} = -N_c \mathrm{Sp}\ \ln\Big[\partial_\tau \ +\ H(U^{\gamma_5}) \ +\ A^\dagger(t)\dot{A}(t) \ -\ i\beta\dot{\vec{Z}}\cdot\nabla \\ +\ \beta A^\dagger(t)(\hat{m}-\bar{m}\mathbf{1})A(t) \ -\ \beta A^\dagger(t)s_\mu\gamma_\mu\hat{Q}_s A(t)\Big] \tag{26}$$

with the angular velocity

$$A^\dagger(t)\dot{A}(t) \ =\ i\Omega_E \ =\ \frac{1}{2}i\Omega_E^a\lambda^a \tag{27}$$

and the velocity of the translational motion

$$\dot{\vec{Z}} \ =\ \frac{d}{dt}\vec{Z}. \tag{28}$$

Hence, Eq. (21) and Eq. (22) can be written in terms of the rotated Dirac operator $i\tilde{D}$ and chiral effective action $\tilde{S}_{eff}$. The functional integral over the pseudoscalar field $U$ is replaced by the path integral which can be calculated in terms of the eigenstates of the Hamiltonian corresponding to the collective action and these Hamiltonians can be diagonalized in an exact manner.

We take into account the rotational $1/N_c$ corrections and $m_s$ corrections up to linear order:

$$\frac{1}{i\tilde{D}} \simeq \frac{1}{\partial_\tau + H} + \frac{1}{\partial_\tau + H}(-i\Omega_E)\frac{1}{\partial_\tau + H} + \frac{1}{\partial_\tau + H}(-\beta A^\dagger[\hat{m}-\bar{m}\mathbf{1}]A)\frac{1}{\partial_\tau + H}. \tag{29}$$

When the $m_s$ corrections are considered, SU(3) symmetry is no more exact. Thus, the eigenfunctions of the collective Hamiltonian are neither in a pure octet nor in a pure decuplet but in mixed states with higher representations:

$$|8,N\rangle \ =\ |8,N\rangle \ +\ c_{\bar{10}}|\bar{10},N\rangle \ +\ c_{27}|27,N\rangle \tag{30}$$

with

$$c_{\bar{10}} \ =\ \frac{\sqrt{5}}{15}(\sigma - r_1)I_2 m_s, \ \ c_{27} \ =\ \frac{\sqrt{6}}{75}(3\sigma + r_1 - 4r_2)I_2 m_s. \tag{31}$$

The constant $\sigma$ is related to the SU(2) $\pi N$ sigma term $\Sigma_{SU(2)} \ =\ 3/2(m_u+m_d)\sigma$ and $r_i$ designates $K_i/I_i$, where $K_i$ stand for the anomalous moments of inertia defined in Ref. [21].

Having carried out a lengthy manipulation (for details, see Ref. [27]), we arrive at our final expressions for the strange vector form factors. The Sachs strange electric form factor $G_E^s$ is expressed as follows (see appendix A for detail):

$$\begin{aligned} G_E^s(\vec{Q}^2) &= (1-\langle D_{88}^{(8)}\rangle_N)\mathcal{B}(Q^2) \\ &+ \langle D_{8a}^{(8)} J_a\rangle_N \frac{2\mathcal{I}_1(Q^2)}{\sqrt{3}I_1} + \langle D_{8p}^{(8)} J_p\rangle_N \frac{2\mathcal{I}_2(Q^2)}{\sqrt{3}I_2} \\ &+ (1-\langle D_{88}^{(8)}\rangle_N) m_s \mathcal{C}(Q^2) \\ &+ \langle D_{8a}^{(8)} D_{8a}^{(8)}\rangle_N \frac{4m_s}{3I_1}\left(I_1\mathcal{K}_1(\vec{Q}^2) - \mathcal{I}_1(\vec{Q}^2)K_1\right) \\ &+ \langle D_{8p}^{(8)} D_{8p}^{(8)}\rangle_N \frac{4m_s}{3I_2}\left(I_2\mathcal{K}_2(\vec{Q}^2) - \mathcal{I}_2(\vec{Q}^2)K_2\right), \end{aligned} \tag{32}$$

$I_i$ and $K_i$ are the moments of inertia and anomalous moments of inertia [21], respectively, $\mathcal{B}$, $\mathcal{I}_i$, and $\mathcal{K}_i$ correspond to the baryon number, moments of inertia, and the anomalous moments of inertia at $Q^2=0$, respectively. From Eq.(32), we can see easily that at $Q^2=0$ the strange electric form factor $G_E^s$ vanishes (note that $\mathcal{C}(Q^2=0)=0$). Making use of the relation $\sum_{a=1}^{8} D_{8a}^{(8)} J_a = -\sqrt{3}Y/2$ and $J_8 = -N_c/(2\sqrt{3})$, we obtain $G_E^s(Q^2=0) = B-Y = S$. Since the net strangeness of the nucleon is zero, $G_E^s$ at $Q^2=0$ must vanish. The final expression of the Sachs strange magnetic form factor is written (see appendix A for detail) by

$$\begin{aligned} G_M^s(\vec{Q}^2) &= \frac{M_N}{|\vec{Q}|}\left[-\frac{\langle D_{83}^{(8)}\rangle_N}{\sqrt{3}}\left(\mathcal{Q}_0(\vec{Q}^2) + \frac{\mathcal{Q}_1(\vec{Q}^2)}{I_1} + \frac{\mathcal{Q}_2(\vec{Q}^2)}{I_2}\right)\right. \\ &+ \langle (D_{88}^{(8)}-1) J_3\rangle_N \frac{\mathcal{X}_1(\vec{Q}^2)}{3I_1} + \langle d_{3pq} D_{8p}^{(8)} J_q\rangle_N \delta_{pq}\frac{\mathcal{X}_2(\vec{Q}^2)}{\sqrt{3}I_2} \\ &- \frac{2m_s}{\sqrt{3}}\langle (D_{88}^{(8)}-1) D_{83}^{(8)}\rangle_N \mathcal{M}_0(\vec{Q}^2) \\ &+ \frac{m_s}{3}\langle D_{83}^{(8)}\rangle_N\left(2\mathcal{M}_1(\vec{Q}^2) - \frac{2}{\sqrt{3}} r_1 \mathcal{X}_1(\vec{Q}^2)\right) \\ &- \frac{m_s}{\sqrt{3}}\langle D_{83}^{(8)} D_{88}^{(8)}\rangle_N\left(2\mathcal{M}_1(\vec{Q}^2) - \frac{2}{3} r_1 \mathcal{X}_1(\vec{Q}^2)\right) \\ &\left. - m_s\langle d_{3pq} D_{8p}^{(8)} D_{8q}^{(8)}\rangle_N \delta_{pq}\left(2\mathcal{M}_2(\vec{Q}^2) - \frac{2}{3} r_2 \mathcal{X}_2(\vec{Q}^2)\right)\right], \end{aligned} \tag{33}$$

## III. RESULTS AND DISCUSSIONS

In order to evaluate Eqs. (32,33) numerically, we follow the Kahana-Ripka discretized basis method [29]. However, note that it is of great importance to use a reasonably large size of the box ($D \approx 10$ fm) so as to get a numerically stable results. The present SU(3) $\chi$QSM (equivalent to SU(3) NJL on the chiral circle) contains four free parameters. Two of them are fixed in the meson sector by adjusting them to the pion mass, $m_\pi = 139$ MeV, the pion decay constant, $f_\pi = 93$ MeV, and the kaon mass, $m_K = 496$ MeV. As for the fourth parameter, *i.e.* the constituent mass $M$ of up and down quarks, values around $M = 420$ MeV have been used because they have turned out to be the most appropriate one for the description of nucleon observables and form factors (see ref. [27]). In fact, $M = 420$ MeV is the preferred value, which is always used in this paper. For the description of the baryon sector, we choose the method of Blotz *et al.* [21] modified for a finite pion mass. The resulting strange current quark mass comes out around $m_s = 180$ MeV. In order to illustrate the effect of the $m_s$ the calculations in the baryonic sector are performed with both $m_s = 0$ and finite $m_s$. One should note that a SU(3)-calculation with $m_s = 0$ does not correspond to a SU(2) calculation, since the spaces, in which the collective quantization are performed, are different.

Figure 1 shows the strange electric form factor $G_E^s(Q^2)$, as the constituent quark mass $M$ is varied from 370 MeV to 450 MeV without $m_s$ corrections. The strange electric form factor $G_E^s$ decreases as $M$ increases. As shown in Fig. 1, the $G_E^s(Q^2)$ without the $m_s$ corrections is rather insensitive to the constituent quark mass $M$. In Fig. 2 the $G_E^s$ with the $m_s$ corrections is drawn. The $m_s$ corrections enhance the $G_E^s$ drastically, contributing to it almost 50%.

The Sachs and Dirac mean-square strange radii are, respectively, defined by

$$\langle r^2 \rangle_s^{Sachs} \;=\; -6 \frac{dG_E^s(Q^2)}{dQ^2} \mid_{Q^2=0}, \quad \langle r^2 \rangle_s^{Dirac} \;=\; -6 \frac{dF_1^s(Q^2)}{dQ^2} \mid_{Q^2=0} \tag{34}$$

We obtain $\langle r^2 \rangle_s^{Sachs} = -0.25$ fm$^2$ and $\langle r^2 \rangle_s^{Dirac} = -0.20$ fm$^2$ without the $m_s$ corrections in case of $M = 420$ MeV and $\langle r^2 \rangle_s^{Sachs} = -0.35$ fm$^2$ and $\langle r^2 \rangle_s^{Dirac} = -0.32$ fm$^2$ with them. As

seen from the above results, the $m_s$ corrections increase the $\langle r^2 \rangle_s$ considerably as in case of the $G_E^s$. However, the mechanism of the enhancement of the $\langle r^2 \rangle_s$ by the $m_s$ corrections is distinguished from that of the $G_E^s$ at finite momentum transfers. Fig. 3 depicts the baryon ($B$) and hypercharge ($Y$) densities with $r^2$. The $m_s$ corrections elevate the baryon density in small $r$ region sizably while they lessen its tail quite much in such a way that the baryon number is always kept to be one. On the other hand, the hypercharge one is almost not changed. Hence, the increase of the baryon density brings about the enhancement of the $G_E^s$, while the suppression of its tail increases the $\langle r^2 \rangle_s$. In fact, we obtain the baryon and hypercharge radii, respectively: $\langle r^2 \rangle_B = 0.48$ fm$^2$, $\langle r^2 \rangle_Y = 0.73$ fm$^2$ without the $m_s$ corrections and $\langle r^2 \rangle_B = 0.35$ fm$^2$, $\langle r^2 \rangle_Y = 0.70$ fm$^2$ with them. As the $m_s$ corrections are switched on, $\langle r^2 \rangle_B$ is almost 30% decreased and yields correspondingly the enhancement of $\langle r^2 \rangle_s$. Fig. 4 illustrates the strange electric densities weighted with $r^2$. As expected from the above discussion, the $m_s$ corrections amplify the strange electric density.

Fig. 5 draws the strange magnetic form factor without the $m_s$ corrections. In contrast to the $G_E^s$, the $G_M^s$ increases slowly with the increasing constituent quark mass apart from the small $Q^2$ region ( below about $Q^2 = 0.2$ GeV$^2$). Fig. 6 shows the $G_M^s$ with the $m_s$ corrections. It increases as $M$ increases in the whole $Q^2$ region. As we can see from the comparison between these two figures, the $G_M^s$ is reduced dramatically with the $m_s$ corrections being considered. In case of $M = 420$ MeV, the $m_s$ corrections bring it down almost by 40%. The strange magnetic moment is defined as the strange magnetic form factor at $Q^2 = 0$. The strange magnetic moment we have obtained is $\mu_s = -0.44\ \mu_N$ in unit of the nuclear magneton. Its absolute value is rather greater than in the other models except for the recent calculation by Leinweber [17]: $\mu_s = -0.75 \pm 0.30\ \mu_N$. Fig. 7 shows the strange magnetic densities with $r^2$.

In table 1, the strange magnetic moments $\mu_s$ and mean-square strange radii $\langle r^2 \rangle_s$ are displayed as a function of $M$ and $m_s$. In table 2, we have made a comparison for the $\mu_s$ and $\langle r^2 \rangle_s^{Sachs}$ between different models.

We want to take the occasion to comment on Ref. [32]. Though Ref. [32] seems to

use the same model as the present work, there are significant differences between these two papers. First, Weigel *et al.* [32] do not consider rotational $1/N_c$ corrections in contrast to the present paper. This has the immediate consequence that the magnetic moments of Weigel *et al.* are $\mu_p = 1.06\ \mu_N,\ \mu_n = -0.69\ \mu_N$ for the nucleon [1] whereas the present work (including those corrections) yields $\mu_p = 2.20\ \mu_N,\ \mu_n = -1.59\ \mu_N$ with a far better comparison with experiment ($\mu_p = 2.79\ \mu_N,\ \mu_n = -1.91\ \mu_N$). Furthermore, Weigel *et al.* regularize, besides the real part of the action, also the imaginary one. This meets problems in producing the anomaly structure and is hence avoided in the approach of the present work. In addition the calculation of Weigel *et al.* are not fully self-consistent but use some scaling approximations.

## IV. SUMMARY AND CONCLUSION

In summary, we have calculated in the SU(3) chiral quark-soliton model ($\chi$QSM) often called the semibosonized SU(3) Nambu–Jona-Lasinio model, the strange electric and magnetic form factors of the nucleon, $G_E^s(Q^2)$ and $G_M^s(Q^2)$ including the strange magnetic moment $\mu_s$, and the mean-square strange radius $\langle r^2\rangle_s$. The theory takes into account rotational $1/N_c$ corrections and linear $m_s$ corrections. We have obtained $\mu_s = -0.44\ \mu_N$, $\langle r^2\rangle_s^{Dirac} = -0.32$ fm$^2$ and $\langle r^2\rangle_s^{Sachs} = -0.35$ fm$^2$. The results have been compared with different other models.

There are several points where the present calculations leave room for further studies. Apparently the dependence of the form factors on the value of $m_s$ is quite noticeable and probably one has to go to higher orders in perturbation theory in $m_s$. The hedgehog ansatz and the embedding of SU(2) into SU(3) cause the asymptotic behavior of the kaon and pion fields to be similar, which might have some influence on the form factors at low momentum transfers. Besides the strange vector form factors the strange axial form factors are also of

[1] For this comparison, the constituent quark mass $M = 450$ MeV is chosen. In case of $M = 420$ MeV, we have obtained $\mu_p = 2.39\ \mu_N$ and $\mu_n = -1.76\ \mu_N$ [24].

great interest. Presently we are performing investigations to clarify these questions.

## ACKNOWLEDGMENT

We would like to thank Chr.V. Christov, P.V. Pobylitsa, M.V. Polyakov and W. Broniowski for fruitful discussions and critical comments. This work has partly been supported by the BMBF, the DFG and the COSY–Project (Jülich).

## APPENDIX A:

In this appendix, we present all formulae appearing in Eqs.(32,33).

$$
\begin{aligned}
\mathcal{B}(\vec{Q}^2) &= \int d^3x\; j_0(Qr) \left[ \Psi^\dagger_{val}(x)\Psi_{val}(x) \;-\; \frac{1}{2}\sum_n \mathrm{sgn}(E_n)\Psi^\dagger_n(x)\Psi_n(x) \right], \\
\mathcal{C}(Q^2) &= -\frac{2N_c}{3}\sum_{nm}\int d^3x j_0(Qr)\int d^3y \left[ \frac{\Psi^\dagger(y)\beta\Psi_{val}(y)\Psi^\dagger_{val}(x)\Psi_n(x)}{E_n - E_{val}} \right. \\
&\qquad \left. + \frac{1}{2}R_{\mathcal{M}}(E_n,E_m)\Psi^\dagger_n(y)\beta\Psi_m(y)\Psi^\dagger_m(x)\Psi_n(x) \right], \qquad \text{(A1)} \\
\mathcal{I}_1(\vec{Q}^2) &= \frac{N_c}{6}\sum_{n,m}\int d^3x\; j_0(Qr)\int d^3y \left[ \frac{\Psi^\dagger_n(x)\vec{\tau}\Psi_{val}(x)\cdot\Psi^\dagger_{val}(y)\vec{\tau}\Psi_n(y)}{E_n - E_{val}} \right. \\
&\qquad \left. +\; \frac{1}{2}\Psi^\dagger_n(x)\vec{\tau}\Psi_m(x)\cdot\Psi^\dagger_m(y)\vec{\tau}\Psi_n(y)\mathcal{R}_{\mathcal{I}}(E_n,E_m) \right], \\
\mathcal{I}_2(\vec{Q}^2) &= \frac{N_c}{6}\sum_{n,m^0}\int d^3x\; j_0(Qr)\int d^3y \left[ \frac{\Psi^\dagger_{m^0}(x)\Psi_{val}(x)\Psi^\dagger_{val}(y)\Psi_{m^0}(y)}{E_{m^0} - E_{val}} \right. \\
&\qquad \left. +\; \frac{1}{2}\Psi^\dagger_n(x)\Psi_{m^0}(x)\Psi^\dagger_{m^0}(y)\Psi_n(y)\mathcal{R}_{\mathcal{I}}(E_n,E^0_m) \right], \\
\mathcal{K}_1(\vec{Q}^2) &= \frac{N_c}{6}\sum_{n,m}\int d^3x\; j_0(Qr)\int d^3y \left[ \frac{\Psi^\dagger_n(x)\vec{\tau}\Psi_{val}(x)\cdot\Psi^\dagger_{val}(y)\beta\vec{\tau}\Psi_n(y)}{E_n - E_{val}} \right. \\
&\qquad \left. +\; \frac{1}{2}\Psi^\dagger_n(x)\vec{\tau}\Psi_m(x)\cdot\Psi^\dagger_m(y)\beta\vec{\tau}\Psi_n(y)\mathcal{R}_{\mathcal{M}}(E_n,E_m) \right], \\
\mathcal{K}_2(\vec{Q}^2) &= \frac{N_c}{6}\sum_{n,m^0}\int d^3x\; j_0(Qr)\int d^3y \left[ \frac{\Psi^\dagger_{m^0}(x)\Psi_{val}(x)\Psi^\dagger_{val}(y)\beta\Psi_{m^0}(y)}{E_{m^0} - E_{val}} \right. \\
&\qquad \left. +\; \frac{1}{2}\Psi^\dagger_n(x)\Psi_{m^0}(x)\Psi^\dagger_{m^0}(y)\beta\Psi_n(y)\mathcal{R}_{\mathcal{M}}(E_n,E^0_m) \right] \qquad \text{(A2)}
\end{aligned}
$$

with regularization functions

$$\mathcal{R}_I(E_n,E_m) = -\frac{1}{2\sqrt{\pi}}\int_0^\infty \frac{du}{\sqrt{u}}\phi(u;\Lambda_i)\left[\frac{E_n e^{-uE_n^2}+E_m e^{-uE_m^2}}{E_n+E_m} \;+\; \frac{e^{-uE_n^2}-e^{-uE_m^2}}{u(E_n^2-E_m^2)}\right],$$
$$\mathcal{R}_{\mathcal{M}}(E_n,E_m) = \frac{1}{2}\frac{\mathrm{sgn}(E_n)-\mathrm{sgn}(E_m)}{E_n-E_m}. \tag{A3}$$

$$\begin{aligned}
\mathcal{Q}_0(\vec{Q}^2) &= N_c\int d^3x j_1(qr)\Big[\Psi^\dagger_{val}(x)\gamma_5\{\hat{r}\times\vec{\sigma}\}\cdot\vec{\tau}\Psi_{val}(x)\\
&\qquad -\frac{1}{2}\sum_n \mathrm{sgn}(E_n)\Psi^\dagger_n(x)\gamma_5\{\hat{r}\times\vec{\sigma}\}\cdot\vec{\tau}\Psi_n(x)\mathcal{R}(E_n)\Big],\\
\mathcal{Q}_1(\vec{Q}^2) &= \frac{iN_c}{2}\sum_n\int d^3x j_1(qr)\int d^3y\\
&\quad\times\left[\mathrm{sgn}(E_n)\frac{\Psi^\dagger_n(x)\gamma_5\{\hat{r}\times\vec{\sigma}\}\times\vec{\tau}\Psi_{val}(x)\cdot\Psi^\dagger_{val}(y)\vec{\tau}\Psi_n(y)}{E_n-E_{val}}\right.\\
&\qquad\left.+\;\frac{1}{2}\sum_m\Psi^\dagger_n(x)\gamma_5\{\hat{r}\times\vec{\sigma}\}\times\vec{\tau}\Psi_m(x)\cdot\Psi^\dagger_m(y)\vec{\tau}\Psi_n(y)\mathcal{R}_{\mathcal{Q}}(E_n,E_m)\right],\\
\mathcal{Q}_2(\vec{Q}^2) &= \frac{N_c}{2}\sum_{m^0}\int d^3x j_1(qr)\int d^3y\\
&\quad\times\left[\mathrm{sgn}(E_{m^0})\frac{\Psi^\dagger_{m^0}(x)\gamma_5\{\hat{r}\times\vec{\sigma}\}\cdot\vec{\tau}\Psi_{val}(x)\Psi^\dagger_{val}(y)\Psi_{m^0}(y)}{E_{m^0}-E_{val}}\right.\\
&\qquad\left.+\;\sum_n\Psi^\dagger_n(x)\gamma_5\{\hat{r}\times\vec{\sigma}\}\cdot\vec{\tau}\Psi_{m^0}(x)\Psi^\dagger_{m^0}(y)\Psi_n(y)\mathcal{R}_{\mathcal{Q}}(E_n,E_{m^0})\right],\\
\mathcal{X}_1(\vec{Q}^2) &= N_c\sum_n\int d^3x j_1(qr)\int d^3y\left[\frac{\Psi^\dagger_n(x)\gamma_5\{\hat{r}\times\vec{\sigma}\}\Psi_{val}(x)\cdot\Psi^\dagger_{val}(y)\vec{\tau}\Psi_n(y)}{E_n-E_{val}}\right.\\
&\qquad\left.+\;\frac{1}{2}\sum_m\Psi^\dagger_n(x)\gamma_5\{\hat{r}\times\vec{\sigma}\}\Psi_m(x)\cdot\Psi^\dagger_m(y)\vec{\tau}\Psi_n(y)\mathcal{R}_{\mathcal{M}}(E_n,E_m)\right],\\
\mathcal{X}_2(\vec{Q}^2) &= N_c\sum_{m^0}\int d^3x j_1(qr)\int d^3y\left[\frac{\Psi^\dagger_{m^0}(x)\gamma_5\{\hat{r}\times\vec{\sigma}\}\cdot\vec{\tau}\Psi_{val}(x)\Psi^\dagger_{val}(y)\Psi_{m^0}(y)}{E_{m^0}-E_{val}}\right.\\
&\qquad\left.+\;\sum_n\Psi^\dagger_n(x)\gamma_5\{\hat{r}\times\vec{\sigma}\}\cdot\vec{\tau}\Psi_{m^0}(x)\Psi^\dagger_{m^0}(y)\Psi_n(y)\mathcal{R}_{\mathcal{M}}(E_n,E_{m^0})\right],\\
\mathcal{M}_0(\vec{Q}^2) &= \frac{N_c}{3}\sum_n\int d^3x j_1(qr)\int d^3y\left[\frac{\Psi^\dagger_n(x)\gamma_5\{\hat{r}\times\vec{\sigma}\}\cdot\vec{\tau}\Psi_{val}(x)\Psi^\dagger_{val}(y)\beta\Psi_n(y)}{E_n-E_{val}}\right.\\
&\qquad\left.+\;\frac{1}{2}\sum_m\Psi^\dagger_n(x)\gamma_5\{\hat{r}\times\vec{\sigma}\}\cdot\vec{\tau}\Psi_m(x)\Psi^\dagger_m(y)\beta\Psi_n(y)\mathcal{R}_\beta(E_n,E_m)\right],\\
\mathcal{M}_1(\vec{Q}^2) &= \frac{N_c}{3}\sum_n\int d^3x j_1(qr)\int d^3y\\
&\quad\times\left[\frac{\Psi^\dagger_n(x)\gamma_5\{\hat{r}\times\vec{\sigma}\}\Psi_{val}(x)\cdot\Psi^\dagger_{val}(y)\beta\vec{\tau}\Psi_n(y)}{E_n-E_{val}}\right.\\
&\qquad\left.+\;\frac{1}{2}\sum_m\Psi^\dagger_n(x)\gamma_5\{\hat{r}\times\vec{\sigma}\}\Psi_m(x)\cdot\Psi^\dagger_m(y)\beta\vec{\tau}\Psi_n(y)\mathcal{R}_\beta(E_n,E_m)\right],
\end{aligned}$$

$$\mathcal{M}_2(\vec{Q}^2) = \frac{N_c}{3}\sum_{m^0}\int d^3x j_1(qr)\int d^3y$$
$$\times\left[\frac{\Psi^\dagger_{m^0}(x)\gamma_5\{\hat{r}\times\vec{\sigma}\}\cdot\vec{\tau}\Psi_{val}(x)\Psi^\dagger_{val}(y)\beta\Psi_{m^0}(y)}{E_{m^0}-E_{val}}\right.$$
$$\left.+\sum_n \Psi^\dagger_n(x)\gamma_5\{\hat{r}\times\vec{\sigma}\}\cdot\vec{\tau}\Psi_{m^0}(x)\Psi^\dagger_{m^0}(y)\beta\Psi_n(y)\mathcal{R}_\beta(E_n,E_{m^0})\right]. \tag{A4}$$

The regularization functions for the $G_M^s$ are

$$\mathcal{R}(E_n) = \int\frac{du}{\sqrt{\pi u}}\phi(u;\Lambda_i)|E_n|e^{-uE_n^2},$$
$$\mathcal{R}_{\mathcal{Q}}(E_n,E_m) = \frac{1}{2\pi}c_i\int_0^1 d\alpha\frac{\alpha(E_n+E_m)-E_m}{\sqrt{\alpha(1-\alpha)}}\frac{\exp\left(-[\alpha E_n^2+(1-\alpha)E_m^2]/\Lambda_i^2\right)}{\alpha E_n^2+(1-\alpha)E_m^2},$$
$$\mathcal{R}_\beta(E_n,E_m) = \frac{1}{2\sqrt{\pi}}\int_0^\infty\frac{du}{\sqrt{u}}\phi(u;\Lambda_i)\left[\frac{E_n e^{-uE_n^2}-E_m e^{-uE_m^2}}{E_n-E_m}\right]. \tag{A5}$$

The cutoff parameter $\phi(u;\Lambda_i) = \sum_i c_i\theta\left(u-\frac{1}{\Lambda_i^2}\right)$ is fixed by reproducing the pion decay constants and other mesonic properties [27].

## TABLES

TABLE I. The strange magnetic moments and mean-square strange radius as varying the constituent quark mass.

| $M$ | 370 MeV | | 420 MeV | | 450 MeV | |
|---|---|---|---|---|---|---|
| $m_s$ [MeV] | 0 | 180 | 0 | 180 | 0 | 180 |
| $\mu_s[\mu_N]$ | $-0.87$ | $-0.37$ | $-0.78$ | $-0.44$ | $-0.74$ | $-0.50$ |
| $\langle r^2\rangle_s^{Dirac}[\mathrm{fm}^2]$ | $-0.22$ | $-0.47$ | $-0.19$ | $-0.32$ | $-0.16$ | $-0.27$ |
| $\langle r^2\rangle_s^{Sachs}[\mathrm{fm}^2]$ | $-0.28$ | $-0.49$ | $-0.25$ | $-0.35$ | $-0.21$ | $-0.31$ |

TABLE II. The theoretical comparison for the strange magnetic moment and mean-square strange radius between different models. $M = 420$ MeV is used for the present work.

| models | $\mu_s[\mu_N]$ | $\langle r^2\rangle_s^{Sachs}[\mathrm{fm}^2]$ | references |
|---|---|---|---|
| Jaffe | $-0.31 \pm 0.09$ | $0.14 \pm 0.07$ | [9] |
| Hammer *et al.* | $-0.24 \pm 0.03$ | $0.23 \pm 0.03$ | [11] |
| Koepf *et al.* | $-2.6 \times 10^{-2}$ | $-0.97 \times 10^{-2}$ | [12] |
| Musolf & Burkhardt | $-(0.31 \to 0.40)$ | $-(2.71 \to 3.23) \times 10^{-2}$ | [13] |
| Cohen *et al.* | $-(0.24 \to 0.32)$ | $-(3.99 \to 4.51) \times 10^{-2}$ | [14] |
| Forkel *et al.* | | $1.69 \times 10^{-2}$ | [18] |
| Park & Weigel | $-0.05$ | 0.05 | [16] |
| Park *et al.* | $-0.13$ | $-0.11$ | [15] |
| Leinweber | $-0.75 \pm 0.30$ | | [17] |
| Alberico *et al.* | $-0.14$ | 0.055 | [31] |
| Weigel *et al.* | $-0.05 \to 0.25$ | $-0.2 \to -0.1$ | [32] |
| SU(3) $\chi$QSM | $-0.44$ | $-0.35$ | Present work |

# REFERENCES


[1] J. Ashman *et al.*, *Nucl. Phys.* **B328** (1989) 1.

[2] B. Adeva *et al.*, *Phys. Lett.* **302B** (1993) 533.

[3] D. Adams *et al.*, *Phys. Lett.* **329B** (1994) 399.

[4] P.L. Anthony *et al.*, *Phys. Rev. Lett.* **71** (1993) 959.

[5] K. Abe *et al.*, *Phys. Rev. Lett.* **75** (1995) 25.

[6] L.A. Ahrens *et al.*, *Phys. Rev.* **D35** (1987) 785.

[7] D.B. Kaplan and A. Manohar, *Nucl. Phys.* **B310** (1988) 527.

[8] G.T. Garvey, W.C. Louis, and D.H. White, *Phys. Rev.* **C48** (1993) 761.

[9] R.L. Jaffe, *Phys. Lett.* **229B** (1989) 275.

[10] G. Höhler, E. Pietarinen, and I. Sabba-Stefanescu, *Nucl. Phys.* **B114** (1976)505.

[11] H.W. Hammer, Ulf-G. Meißner, and D. Drechsel, TK-95-24 [`hep-ph/9509393`] (1995).

[12] W. Koepf, E.M. Henley and S.J. Pollock, *Phys. Lett.* **288B** (1992) 11.

[13] M.J. Musolf and M. Burkardt, *Z. Phys.* **C61** (1994) 433.

[14] T.D. Cohen, H.Forkel and M. Nielsen, *Phys. Lett.* **B316** (1993) 1.

[15] N.W. Park, J. Schechter, and H. Weigel, *Phys. Rev.* **D43** (1991) 869.

[16] N.W. Park and H. Weigel, *Nucl. Phys.* **A541** (1992) 453.

[17] D.B. Leinweber, DOE/ER/40427-27-N95 [`hep-ph/9512319`] (1995).

[18] H. Forkel, M. Nielsen, X. Jin and T.D. Cohen, *Phys. Rev.* **C50** (1994) 3108.

[19] M.J. Musolf *et al.*, *Phys. Rep.* **239** (1994) 1.

[20] E.J. Beise and R.D. McKeown, *Comments Nucl. Part. Phys.* **20** (1991) 105.

[21] A. Blotz, D. Diakonov, K. Goeke, N.W. Park, V. Petrov and P.V. Pobylitsa, *Nucl. Phys.* **A555** (1993) 765.

[22] H. Weigel, R. Alkofer and H. Reinhardt, *Nucl. Phys.* **B387** (1992) 638.

[23] A. Blotz, M. Praszałowicz, and K. Goeke, *Phys. Rev.* **D53** (1996) 485.

[24] H.-C. Kim, M. Polyakov, A. Blotz, and K. Goeke, RUB-TPII-6/95 [hep-ph/9506422], Nucl. Phys. A in press (1996).

[25] H.-C. Kim, A. Blotz, M. Polyakov, and K. Goeke, *Phys. Rev.* **D53** (1996) 4013.

[26] H.-C. Kim, A. Blotz, C. Schneider, and K. Goeke, *Nucl. Phys.* **A596** (1996) 415.

[27] Chr. V. Christov, A. Blotz, H.-C. Kim, P. Pobylitsa, T. Watabe, Th. Meissner, E. Ruiz Arriola, and K. Goeke RUB-TPII-32/95, *Prog. Nucl. Part. Phys.* **37** to be published (1996).

[28] D. Diakonov and V. Petrov, *Nucl. Phys.* **B272** (1986) 457.

[29] S. Kahana and G. Ripka, *Nucl. Phys.* **A429** (1984) 462.

[30] H. Weigel, R. Alkofer and H. Reinhardt, *Nucl. Phys.* **B387** (1992) 638.

[31] W.M. Alberico, S.M. Bilensky, C. Giunti and C. Maieron, DFTT48/95 [hep-ph/9508277] (1995).

[32] H. Weigel, A. Abada, R. Alkofer, and H. Reinhardt, *Phys. Lett.* **353B** (1995) 20.

# Figure Captions

**Fig. 1**: The strange electric form factor $G_E^s$ as functions of $Q^2$ without the $m_s$ corections: The solid curve corresponds to the constituent quark mass M=420 MeV, while dot-dashed curve draws M=370 MeV. The dashed curve displays the case of M=450 MeV. The M=420 MeV is distinguished since all other observables of the nucleon are then basically reproduced in this model.

**Fig. 2**: The strange electric form factor $G_E^s$ as functions of $Q^2$ with $m_s = 180$ MeV: The solid curve corresponds to the constituent quark mass M=420 MeV, while dot-dashed curve draws M=370 MeV. The dashed curve displays the case of M=450 MeV. The M=420 MeV is distinguished since all other observables of the nucleon are then basically reproduced in this model.

**Fig. 3**: The baryon and hypercharge densities as functions of $r$. The solid curve draws the baryon charge density with $m_s = 180$ MeV while the dashed one for the same density without the $m_s$ corrections. The dot-dashed curve designates the hypercharge density with $m_s = 180$ MeV while the dot-dot-dashed one for the same density without the $m_s$ corrections. The constituent quark mass $M = 420$ MeV is used.

**Fig. 4**: The strange electric density $r^2\rho_E^s$ as functions of $r$: The solid curve draws the $r^2\rho_E^s$ with $m_s = 180$ MeV, whereas the dashed one displays it without the $m_s$ corrections. The constituent quark mass $M = 420$ MeV is used.

**Fig. 5**: The strange magnetic form factor without the $m_s$ corrections as a function of $Q^2$: The solid curve corresponds to the constituent quark mass $M = 420$ MeV, while dashed curve draws the case of M = 450 MeV. The dot-dashed curve displays the case of M = 370 MeV. The strange quark mass is taken to be $m_s = 0$. The M=420 MeV is distinguished

since all other observables of the nucleon are then basically reproduced in this model.

**Fig. 6**: The strange magnetic form factor with $m_s = 180$ MeV as a function of $Q^2$: The solid curve corresponds to the constituent quark mass $M = 420$ MeV, while dashed curve draws the case of M = 450 MeV. The dot-dashed curve displays the case of M = 370 MeV. The strange quark mass is taken to be $m_s = 180$ MeV. The M=420 MeV is distinguished since all other observables of the nucleon are then basically reproduced in this model.

**Fig. 7**: The strange magnetic density $r^2\rho_M^s$ as functions of $r$: The solid curve draws the $r^2\rho_M^s$ with $m_s = 180$ MeV, whereas the dashed one displays it without the $m_s$ corrections. The constituent quark mass $M = 420$ MeV is used.

# Figures

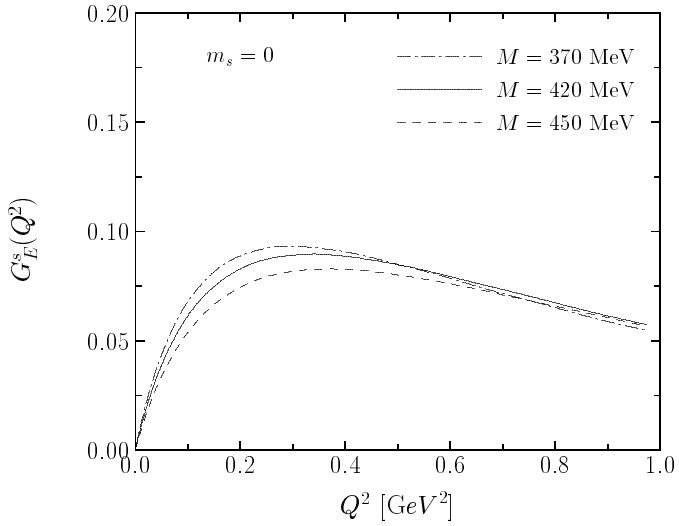


**Figure 1**

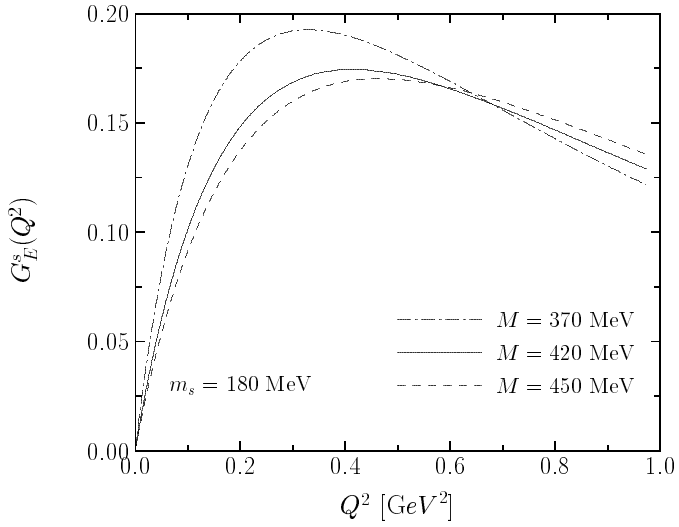


**Figure 2**

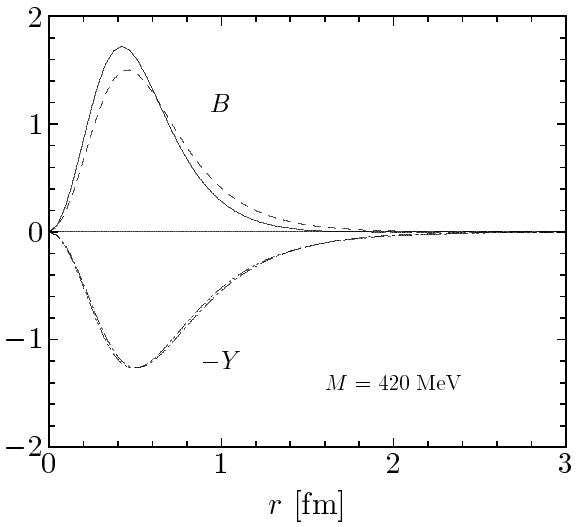


**Figure 3**

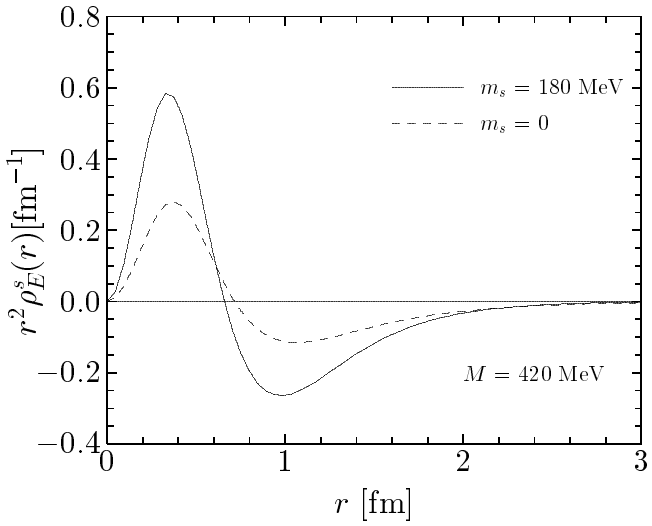


**Figure 4**

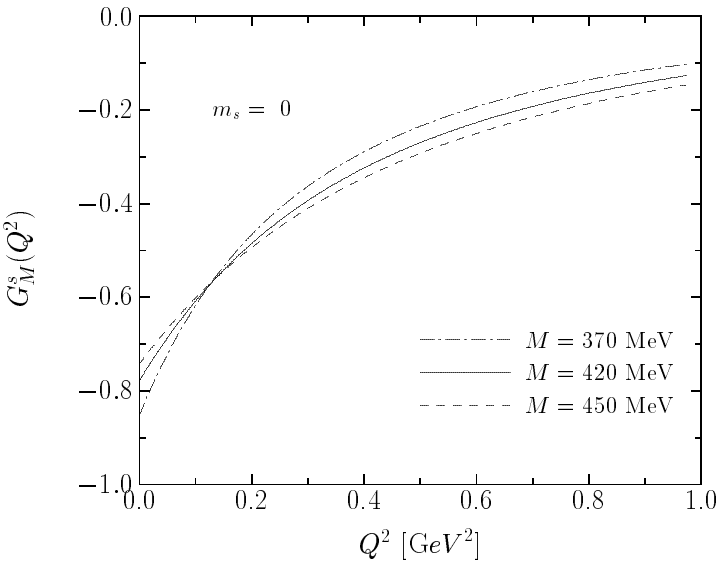


**Figure 5**

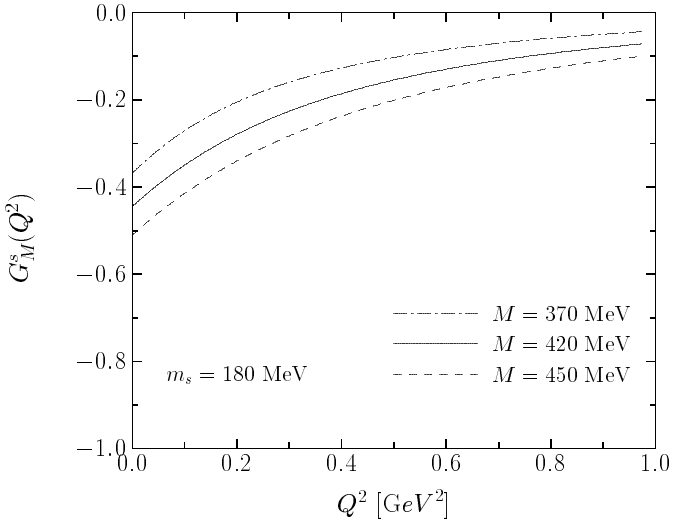


**Figure 6**

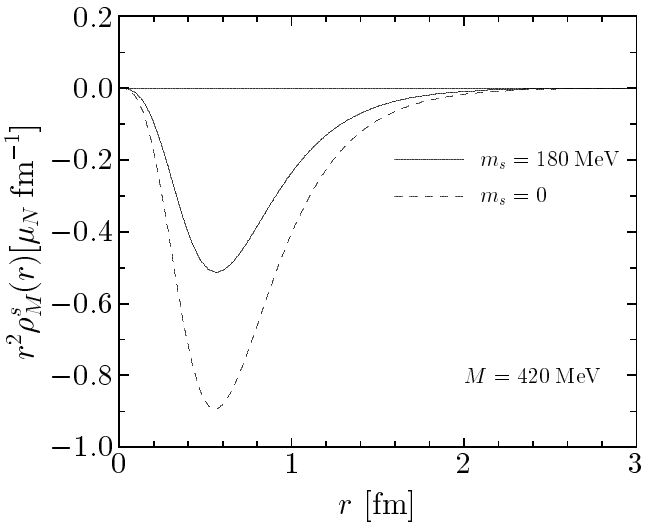
0.2
0.0
−0.2
−0.4
−0.6
−0.8
−1.0
0
1
2
3
$r^2\rho_M^s(r)[\mu_N\,\mathrm{fm}^{-1}]$
$r$ [fm]
$m_s = 180$ MeV
$m_s = 0$
$M = 420$ MeV

**Figure 7**